Engineering Research Express

INCLUSIVE PUBLISHING TRUSTED SCIENCE

PURPOSE-LED PUBLISHING™

PAPER • **OPEN ACCESS**

A study of XLPE insulation failure in power cables under electromagnetic stress

To cite this article: Babu Naik Gugulothu *et al* 2024 *Eng. Res. Express* **6** 035352

View the article online for updates and enhancements.

You may also like

- Effects of electrical aging on the structural and physicochemical properties of crosslinked polyethylene (XLPE) cable insulation material
Abdallah Hedir, Ferhat Slimani, Mustapha Moudoud et al.
- A deterministic breakdown model for dielectric interfaces subjected to tangential electric field
Emre Kantar and Sverre Hvidsten
- Assessment of UV-Aging of Crosslinked Polyethylene Cable Insulation by Electrical Measurements, FTIR and DSC Analyses
Abdallah Hedir, Sébastien Rondot, Omar Jbara et al.

This content was downloaded from IP address 188.119.23.237 on 10/08/2025 at 19:11

Engineering Research Express

PAPER

A study of XLPE insulation failure in power cables under electromagnetic stress

Babu Naik Gugulothu[1], **Sanjay Lakshminarayanan**[1], **Madhu Palati**[1], **Suresh Haleyur Lakshmegowda**[2] and **Mahipal Bukya**[3]

[1] Department of Electrical and Electronics Engineering, BMS Institute of Technology and Management, Visvesvaraya Technological University, Belagavi, 590018, Karnataka, India
[2] Department of Electrical and Electronics Engineering, Sir M. Visvesvaraya Institute of Technology Visvesvaraya Technological University, Belagavi, 590018, Karnataka, India
[3] Department of Electrical and Electronics Engineering, Manipal Institute of Technology Bengaluru, Manipal Academy of Higher Education, Manipal, India

E-mail: mahipal.bukya@manipal.edu

Keywords: MV XLPE cables, finite element method, electric field stress, cables, defect, electric field, electric potential

OPEN ACCESS

RECEIVED
13 April 2024

REVISED
25 August 2024

ACCEPTED FOR PUBLICATION
27 August 2024

PUBLISHED
4 September 2024

Original content from this work may be used under the terms of the Creative Commons Attribution 4.0 licence.

Any further distribution of this work must maintain attribution to the author(s) and the title of the work, journal citation and DOI.

Abstract

Underground cables with cross-linked polyethylene (XLPE) insulation are integral to medium voltage (MV) power transmission systems, ensuring continuous electricity supply amidst operational challenges and environmental conditions. However, the reliability of these cables can be compromised over time due to aging and installation-related factors, particularly at joints and terminations. This study offers a comprehensive analysis of how various defects, including spherical air voids, pinholes, and irregularities in semiconducting layers, affect electric field and potential distributions within cable end terminations using COMSOL Multiphysics software. Through detailed simulations, the study identifies significant variations in electric field strength caused by these defects, highlighting critical stress concentration areas. In this study, it assumed that the cable and termination have the same cross-section. By analyzing these simulations, the study provides insights into optimizing cable design and installation practices to enhance the reliability and lifespan of underground power transmission systems. This study introduces a novel approach by combining advanced COMSOL Multiphysics simulations with a detailed analysis of defect impacts on electric field distributions, offering new insights into stress concentrations and degradation at cable terminations. Simulation outcomes reveal significant variations in electric field strengths due to air voids and pinholes in cables and terminations: for 2 mm voids, up to 2.45×10^6 V mm^{-1} near the conductor and 56.5 V mm^{-1} at termination. These findings enhance the understanding of XLPE-insulated cable behavior under electromagnetic stress, providing a basis for mitigating failures and improving overall system performance.

Nomenclature

XLPE	Cross-linked polyethylene
MV	Medium Voltage
FEM	Finite Element Method
PD	Partial Discharge
AC	Alternating Current
DC	Direct Current
HV	High Voltage
PV C	Polyvinyl Chloride
KV	Kilo Voltage
RBF	Radial Basis Function

© 2024 The Author(s). Published by IOP Publishing Ltd

mm	millimeter

Abbreviations List

ϵ_0	Permittivity of free space
ϵ_r	Relative permittivity
ρ_s	space charge density
E	Electric Field
∇V	Potential Gradient
nD_1 *and* nD_2	electric displacement with normal components
V_{ph1}	Single phase voltage
V_0	Output voltage
$\epsilon_{r,Air}$	Relative permittivity in the air
$\epsilon_{r,Insulation}$	Relative permittivity for the insulation.
E_{Air}	Electric field in the air

1. Introduction

Underground cables are an essential component of the power transmission system used by the electric grid [1–6]. The reliability of the transmission system is contingent upon the condition of the power cables. Over time, aging can compromise the insulation's effectiveness, partially or completely, due to factors such as electrical stresses, chemical exposure, mechanical strain, environmental conditions, and operational constraints. These factors collectively contribute to the potential degradation of the insulation system, impacting the overall reliability of the transmission infrastructure [7–11]. Underground cable problems are the primary source of the majority of power outages. Joints and cable termination are essential cable network components. Several studies [12–15] have concluded that cable accessories fail more frequently than the cable itself. Figure 1 [16] and figure 2 are pictures of the cable end termination failure. Cable junction denotes a pivotal location where two or more cables are interconnected or terminated, typically involving specialized components like termination kits or junction boxes. These junctions constitute crucial points within power transmission systems, ensuring essential functions such as electrical continuity, robust insulation, and mechanical support. The functionality, which reduces and balances localized electrical stressors, also makes them prone to failure. The proper material selection, meticulous design, and highly experienced labour for installation are responsible for achieving this delicate equilibrium in electrical stresses. Any deviation or variation could cause an imbalance in the electrical stresses, resulting breakdowns. According to recent statistics on accessory failures during operation, installation is the primary cause (accounting for more than 50%), followed by production and design flaws, contributing significantly to testing failures [17]. The conclusion that installation errors are the main cause of accessory failures is supported by the study of cable termination failures reported in this work. According to this study, transmission and distribution utilities frequently reported failures of cable end terminations.

In [18], Arikan *et al* explored different shapes like equal area, cubic, sphere, and tetrahedrons, which were considered for electric field analysis. Magnetic field analysis is carried out on XLPE cables with balanced and unbalanced loads. The causes of the cable's malfunction were investigated, and the impact of each component on the distribution of the magnetic and electric fields was demonstrated. An electric field study was conducted on a $1 \times 240/25\ mm^2$ cable, using various geometric shapes to analyze their impact on the electric field distribution. For both balanced and unbalanced load scenarios, the magnetic field study was carried out on $3 \times (1 \times 240/25)\ mm^2$ and $3 \times 240/25\ mm^2$ cables with XLPE insulation. M Florkowski [19] described the insulating material characteristics that affect PD at DC voltage. The circumstances of partial discharges (PD) start and post-discharge processes at DC voltage were suggested as modifications to the conventional model. The study was conducted on two types of dielectric materials found in power cables. The influences of the material resistivity on the PD activity were revealed by designing different combinations of specimens. The effect of the void adjacent material resistance on the DC voltage partial discharge inception voltage threshold was a significant result. The dielectric substance surrounding the vacuum has a crucial role in the dynamics of partial discharge, as proved by experiments, even with the model's numerous simplifications. Boudjella *et al* [20] performed a study to demonstrate a numerical modeling of the magnetic field of a 400 kV underground power line that was buried and utilized as a revolutionary prototype at a short distance in different nations. The underground power line was investigated with temporal variation utilizing finite element resolution while current harmonics were present at different places using Comsol Multiphysics with MATLAB software in two

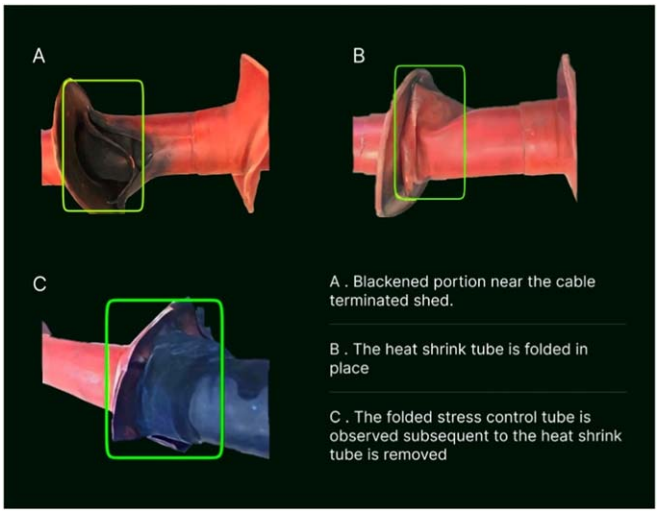


Figure 1. A punctured cable.



Figure 2. Punctured cable near to the cable termination.

dimensions. The simulation findings show how the magnetic flux density varies with various real harmonics rates, both in terms of distribution and amplitude. The impacts of harmonics have an impact on the magnetic field and subsurface cable performance. Bakri *et al* [21] employed the 2D electrostatic COMSOL Multiphysics software, which was based on the finite element approach in ac/dc. Their investigation demonstrated the impact of various cavity shapes on the performance of electrical wires. They considered both the presence and absence of heterogeneous cavities as they investigated the potential and distribution of an electric field in a high-voltage cable model. Medoukali and Zegnini [22] utilized numerical simulation to examine the impact of micro cavity density and arrangement on the electromechanical and electrical restrictions in MV cable XLPE insulation. The MATLAB-based finite element method (FEM) solution of Laplace's equation served as the foundation for the simulation. Both the micro cavity elongation and the electrostatic pressure were calculated. As a result of this elongation, a microchannel emerges, grows as a result of partial discharges to arborescence, and eventually the cable breaks down. The electromechanical limitations were ascertained for various micro cavity configurations and densities.

Elaggoune *et al* [23] conducted a dissolved gas analysis to assess the electrical cable terminations' condition and detect partial discharges within them. They employed Radial Basic Functions (RBF) neural networks as a simulation tool to address this issue, concluding that RBF networks effectively monitor partial discharges in cable terminations. The study also investigated the impact of space charge and cavities within cross-linked polyethylene (XLPE) insulation on potential and electric field distributions. It was determined that voids closer to the conductor have a greater influence, particularly when their size is larger. According to Arabul and Kumru [24], it is crucial to maintain cables within their rated working parameters to avoid additional heat stress that could damage their insulation. While cables are designed to operate at these rated parameters, overloading can cause excessive thermal stress, which accelerates insulation aging and reduces the cable's lifespan. In their investigation, thermal evaluations were performed under various loading scenarios on a 3-phase, 220 kV HVAC,

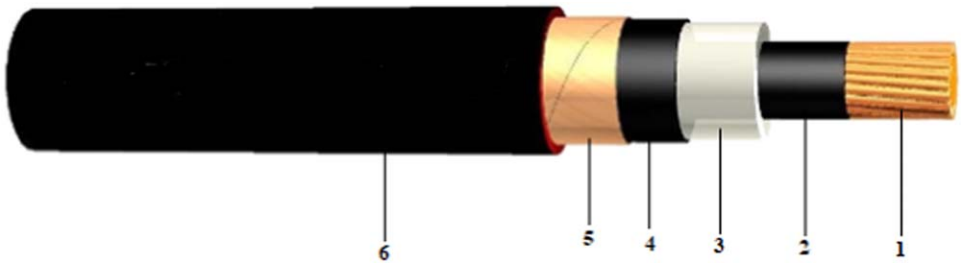


Figure 3. Cross-sectional parts of XLPE cable.

XLPE-insulated undersea cable. The results showed that loading rate, phase imbalance, and seawater temperature had a substantial influence on the cable's maximum temperature, current carrying capability, and overall losses. Experimental analysis of the flashover process was conducted, and simulations using COMSOL Multiphysics software [25–28] modeled potential and electric field distributions under 50 Hz voltage application. These studies considered defects such as spherical air voids, cylindrical pinholes and partial semiconductor layers on XLPE. Additionally, the effect of temperature rise on cable life was studied in papers [29, 30]. Elevated cable temperatures degrade insulation life, potentially leading to cable failure.

In this study, COMSOL Multiphysics software simulates the effects of various defects possibly caused by improper workmanship. These defects include spherical air voids, cylindrical pinholes and partial and semiconductor layer remnants on XLPE. The study compares variations in electric field, potential, and magnetic fields between the cable end termination kit and the armored cable. Unlike the cable, the termination kit lacks armor, causing discontinuities in the electric field inside. COMSOL Multiphysics are used to visualize electromagnetic fields, including electrical circuits, magnetic fields, and electrostatics, within the cable end terminations. A test circuit in COMSOL applies a rated single-phase-to-ground voltage (19.05 kV) and 366 Amps, reflecting real-world feeder currents. The presence of voids and electromagnetic field variations results in volumetric losses, leading to thermal stresses in the cable. These stresses elevate cable temperatures, ultimately risking cable failure. This study is novel for its comprehensive analysis of defects in XLPE-insulated power cables using advanced COMSOL Multiphysics simulations. It uniquely combines the study of various defect types including spherical air voids and pinholes with their effects on electric fields and potential distributions, particularly focusing on cable terminations. Applying realistic operational conditions provides actionable insights for optimizing cable design and installation, enhancing reliability and longevity in real-world power transmission systems.

The research's subsequent sections are organized as follows: The wire utilised in this investigation is briefly described in section 2 along with its materials, construction, and electrostatics modelling. Types of flaws taken into consideration are shown in section 3. In section 4, the results and discussion of different types of voids are given. Section 5 presents the findings from several simulations (both without and with flaws) run on the cable to examine how the position of the heterogeneous cavity affects the electric potential and electric field through mathematical verification.

2. XLPE cable description and methods

The single-phase XLPE medium voltage cable (33 kV), which is frequently used in medium voltage power transmission, was employed in the current study.

2.1. XLPE power cable structure

The XLPE cable's construction is represented in figure 3, and its components are as follows: The cable consists of the following components: (1) a copper conductor, (2) a semi-conducting layer, (3) XLPE for insulation, (4) a semi-conducting shield, (5) a copper tape screen that serves as an earth conductor, and (6) a PVC ground outer sheath. Figure 3 presents the cross-sectional parts of XLPE cable.

Regarding the simulation work, the XLPE cable's size, conductivity, and relativity permeability are considered and are presented in tables 1 and 2. The material properties and geometrical specifications of the XLPE cable are shown in tables 1 and 2.

2.2. COMSOL multiphysics method

The partial differential equations (PDEs) that characterize the issue under study are solved by the computer program COMSOL Multiphysics using finite element techniques [21]. The steps involved are as below:

Table 1. The geometrical properties.

Components	Parameters
Diameter of the Conductor	25 mm
Cross-Sectional Area	490.87 mm^2
Thickness of semiconductor screen	0.5 mm
Thickness of the Insulation	10 mm
Thickness of the outer sheath	2.04 mm
Thickness of the Earthing screen	0.8 mm
Thickness of the Bedding	1.3 mm
Diameter of the Armour wire	2.0 mm
Overall diameter	58.6 mm

Table 2. Properties of the cable material.

Material	Conductivity (S/m)	Relativity permittivity
Copper	58.8×10^6	1
XLPE	10^{-15}	2.3
Aluminum	35.7×10^6	2.2

Step 1: Construct the physical model

Create a detailed geometric model of the XLPE cable, including components such as the copper conductor, semi-conducting layers, XLPE insulation, and outer sheath. The model also includes defects like spherical air voids and pinholes within the insulation and termination regions. Define the cable's geometry by inputting the x and y coordinates of each point. Utilize COMSOL's geometry tools to accurately represent the cross-sectional areas and dimensions listed in table 1.

Step 2: Set material properties and boundary conditions

Assign material properties to the different components of the cable. Input the conductivity and relative permittivity for materials such as copper, XLPE, and air as specified in table 2. Specify boundary conditions to reflect the electrical environment. Apply high voltage and ground conditions to the cable boundaries as per the simulation setup. Define the material interfaces and the presence of defects to study their impact on electric field distributions.

Step 3: Generate the mesh

Create an automated mesh using COMSOL's meshing tools. Select appropriate settings such as free quad meshing and element size parameters to ensure an accurate representation of the geometry, especially around defects and terminations. Adjust the mesh density to capture variations in the potential distributions and electric field effectively.

Step 4: Perform the simulation

Define the solver sequence for stationary analyses to calculate the electric field and potential distributions. Use COMSOL's default solver settings or customize them as needed to handle the complexities introduced by defects and material interfaces. Conduct simulations to assess how defects affect electric field strength and stress concentrations within the cable and its terminations.

2.3. Mathematical model of electrostatic fields

The software COMSOL Multiphysics implements a three-dimensional model. The FEM, which builds a mesh of various elements from the intended model, is its basis. It is used to compute the values at each position in the model to get superior results. The software bundle consists of numerous modules. In the current work, the potential and electric field distributions in the cable, including heterogeneous cavities, were determined by incorporating an electrostatic subdivision into the AC/DC module. In order to investigate the effects of void presence on the XLPE electrical field insulation system, the model cable insulation is also equipped with an air-filled void. In relation to the single-phase XLPE cable field model, a mathematical field model for the distribution of the electrical field in the air-filled gaps is developed.

Poisson's equation and potential gradient are solved using COMSOL's electrostatic application modes with subdomain settings [20]

$$-\nabla.\left(\varepsilon_o \,.\, \varepsilon_r \,.\, \nabla V\right) \;=\; \rho \tag{1}$$

The electrical field is obtained from the potential gradient as

$$E = -\nabla V \tag{2}$$

Where, permittivity of free space is denoted by ε_0, the relative permittivity of applied material is denoted as ε_r and ρ denote the space charge density.

In the electrostatic model, the boundary condition of the contact interaction between two distinct medium has the following mathematical expression:

$$n.\,[Medium_1(D_1) - Medium_2(D_2)] = \rho_s \tag{3}$$

Where, $n.Medium_1(D_1)$ and $n.Medium_2(D_2)$ are the normal components of electric displacement of the two different medium and ρ_s denote the surface charge density.

The sinusoidal input voltage supplied to the electric-potential XLPE cable at the boundary condition is as follows:

$$V_{ph1} = V_0 \sin(\omega t)\ ;\ V_0 = 19.05\ kV \tag{4}$$

At ground level, the sheath boundary potential equals zero ($V = 0$).and the ground boundary medium is as follows:

The electric displacement's normal component is continuously applied over the sheath boundary.

$$n.\,[Medium_1(D_1) - Medium_2(D_2)] = 0 \tag{5}$$

For carrying out the electromagnetic field distribution study the following Maxwell equations are used in COMSOL software,

It is the law of conservation of electric charge, which has

$$\nabla.J = 0 \tag{6}$$

Electric currents generate magnetic fields and are described by

$$\nabla \times H = J \tag{7}$$

Magnetic fields can be expressed as a curl of a vector potential,

$$B = \nabla \times A \tag{8}$$

Electric potentials and time varying magnetic potentials give rise to electric fields,

$$E = -\nabla V - j\omega A \tag{9}$$

In any conducting medium, the current density can be given as

$$J = \sigma E + j\omega D + \sigma v \times B + J_e \tag{10}$$

Where, Current density vector denotes by J, σ is the Electrical conductivity, D denotes the Electric displacement field vector, related to the electric field by $D = \epsilon E$, ω represents the Angular frequency, v is the Velocity of moving charges, Magnetic flux density denotes by B, A is the magnetic potentials and J_e is the External current density vector.

In the present study, frequency domain study available in the COMSOL software is used to simulate the real-time operating conditions.

2.4. Test circuit

The test circuit of XLPE cable is shown in figure 4 [31]. In this model, P_0 represents the losses of the cable conductor, while P_1 indicates the dielectric losses of the XLPE insulation. P_2 encompasses the losses of the metal sheath, including eddy current loss and circulating current loss. T_1 and T_2 specifies the cable conductor's surface temperature and XLPE insulation, and T_s specifies the cable's surface temperature in real time. The thermal resistance components are denoted as R_0 for the cable conductor, R_1 for the XLPE insulation, R_2 for the wrap layer, and R_3 for the outer sheath. Additionally, the heat capacity components are represented by R_4 for the cable conductor, C_1 for the XLPE insulation, C_2 for the wrap layer, and C_3 for the outer sheath.

3. Models of heterogeneous cavities

This paper addressed heterogeneous cavities in terms of content, size, and shape in our work. A cable end termination model is built in COMSOL Multiphysics software using the data given in tables 1 and 2. The length of the cable end termination is taken as 3 meters. The COMSOL model of XLPE cable is illustrated in figure 5 [32]. The centermost part is the copper core surrounded by the inner semi-conductive layer. Then comes the XLPE layer followed by the outer semi-conductive layer and copper shielding layer. The cable termination model is presented in figure 6. The components are labeled as follows: 1 indicates the cable conductor, 2

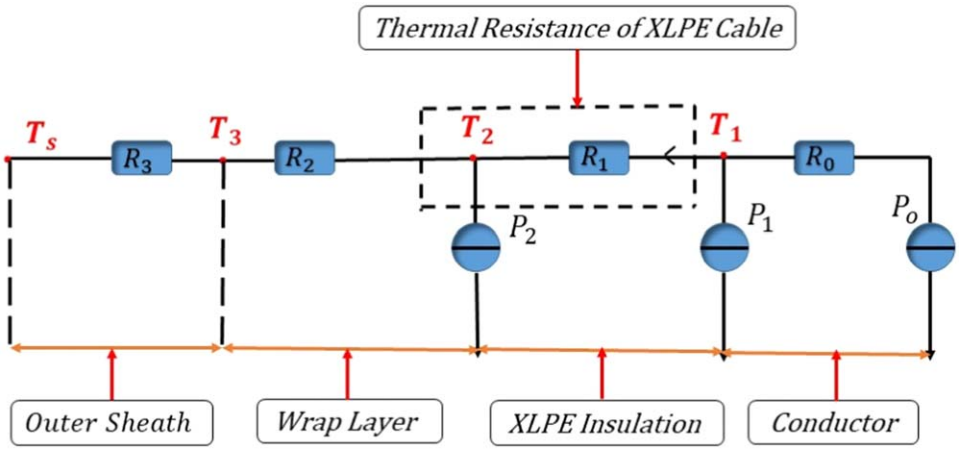


Figure 4. Test circuit of XLPE cable.

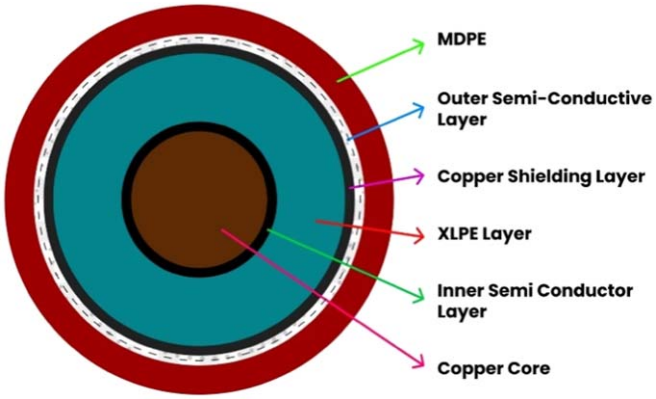


Figure 5. COMSOL model of XLPE cable.

represents the inner semiconducting layer, 3 denotes the cable insulation, 4 identifies the outer semiconducting layer, 5 marks the cable copper shield, 6 shows the stress control tube, and 7 labels the cable jacket.

3.1. Air void cavity

As illustrated in figure 7, a 2 mm air void chamber was created on top of the conductor and placed into the XLPE insulation. The relative permittivity of 1 and conductivity of 8×10^{-15} S m^{-1} are the characteristics of the air.

3.2. Pin Hole cavity

As shown in figure 8, a pinhole cavity was inserted into the XLPE insulation of the conductor. The cavity had a radius of one mm and a height of eight mm. The relative permittivity of 1 and the conductivity of 8×10^{-15} S m^{-1} define the characteristics of the air.

3.3. Partial semiconductor layer

The partial existence of a semiconducting layer on the top of the XLPE insulation was cited as one of the causes of the failure of the cable end termination [13]. This was indicated as one of the reasons for the failure. A simulation of the same impact is carried out with the help of the Comsol Multiphysics software, as indicated by figure 9.

4. Simulation results and discussions

Using COMSOL Multiphysics software, a sinusoidal voltage of 33 kV and 50 Hz frequency was applied to the conductor to simulate the electric field and equipotential distributions within the cable and cable end termination. The simulation also investigates the impact of different types of cavities on the failure of cable end

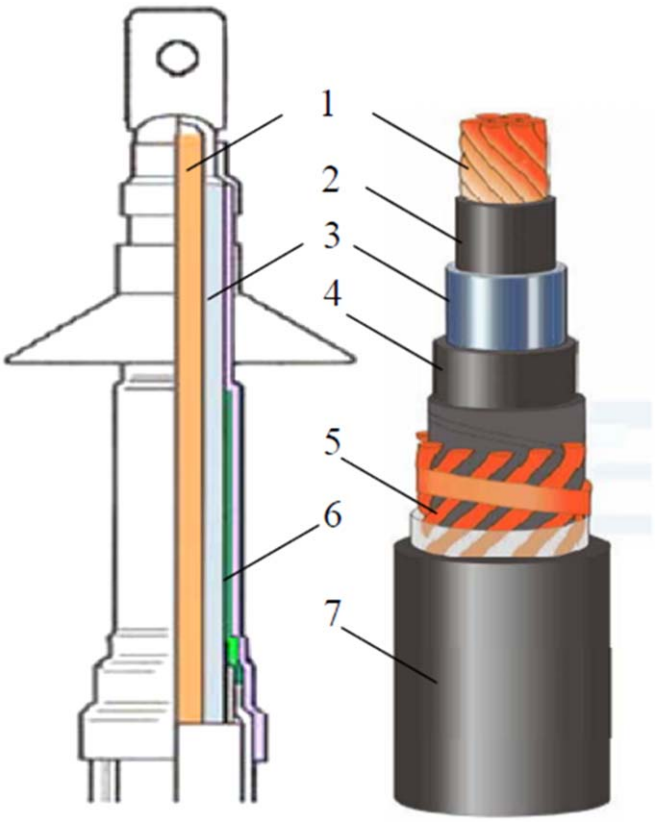


Figure 6. Cable termination model.

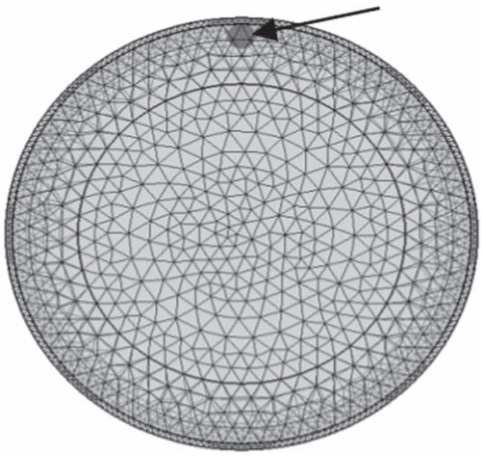


Figure 7. Cable 2D mesh model, highlighting the air void cavity with an arrow.

termination. Results comparing scenarios without cavities and with cavities containing spherical air voids, pinholes, and semiconducting layers on top of XLPE insulation are presented in the following section.

4.1. Case of no cavities

Figure 10 illustrates the electric field and potential distribution within the cable at a frequency of 50 Hz. The circular contours represent the variation of electric potential, increasing from the outer boundary towards the cable's center, suggesting a higher charge concentration in the central region. The electric field norm contours indicate the strongest field intensities near the cable's inner and outer surfaces, gradually decreasing towards the center. These findings suggest a high-voltage cable with potential implications for cable design, insulation optimization, and electrical stress analysis. The rotational symmetry of the electric field surrounding the conductor is observed, as anticipated from the symmetrical arrangement of the wire. Figure 11 depicts the

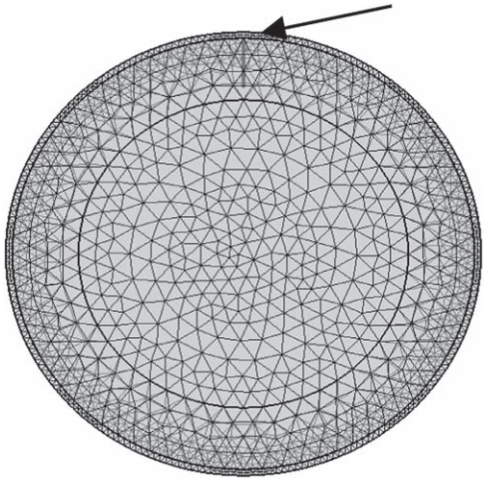


Figure 8. 2D mesh model of a cable, highlighting the pin-hole-sized cavity with an arrow.

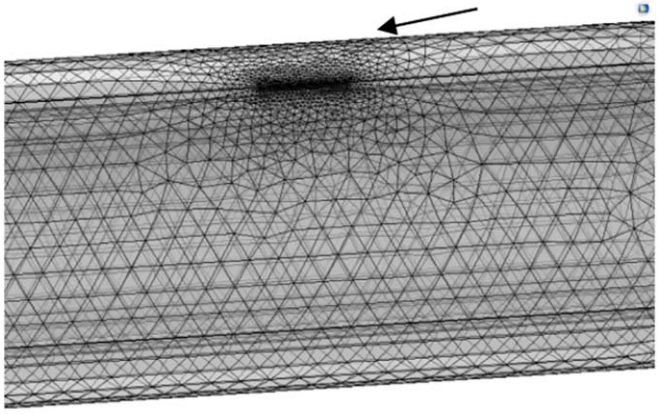


Figure 9. 2D mesh model of a cable, highlighting the partial semiconducting layer with an arrow.

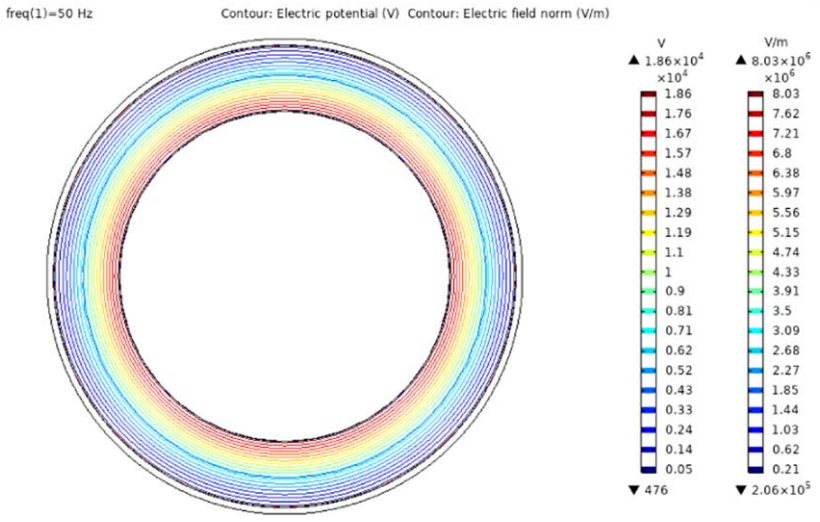


Figure 10. Electric field and potential distribution inside the cable.

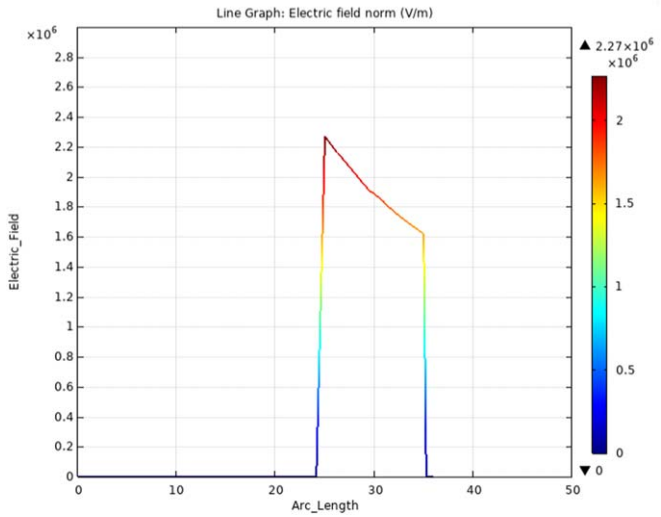


Figure 11. Variation of electric field with radius of the cable.

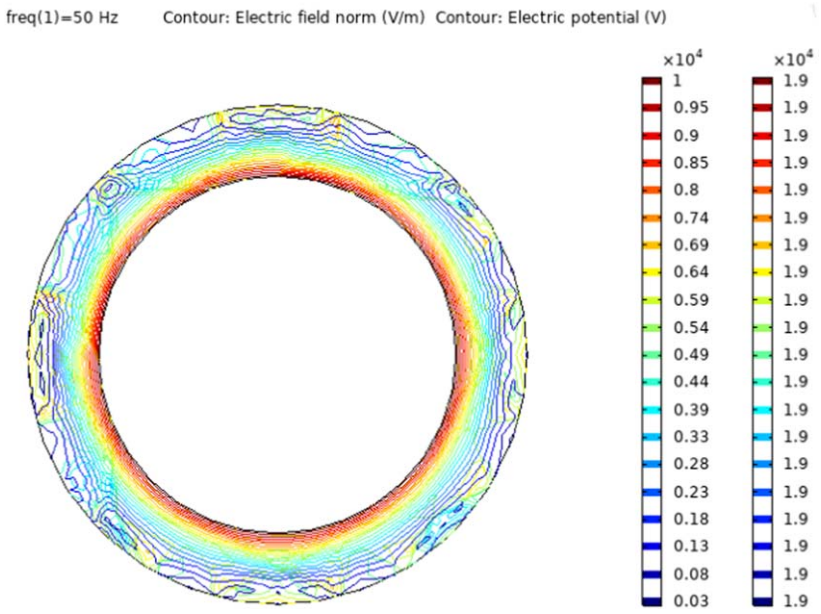


Figure 12. Distribution of electric fields and potentials within the cable end termination.

variation of the electric field with the radius of the cable. The electric field is observed to be highest near the cable's center and gradually decreases towards the outer boundary. This non-uniform distribution has potential implications for cable performance and requires further investigation with detailed material and operational data.

Figure 12 depicts the electric field distribution within the cable end termination. A significant electric field concentration is observed at the termination point, reaching approximately $6.5 \times 10^3\ V/m$. This non-uniform distribution highlights the critical role of cable termination design in mitigating electrical stress and ensuring reliable cable performance. Due to the symmetry of the cable, the rotational symmetry of the electric field surrounding the conductor is observed. As seen in Fig13, the electric field strength reaches a maximum value of 10 kV mm^{-1} around the conductor and remains high near the end of the cable insulation. Since the cable end termination is typically grounded and lacks nearby armor, it results in a significant electric field.

4.2. Case of presence of cavities

For this case study involving the presence of cavities, particularly with spherical air voids and pinhole cavities, the cable junction has a vital part in understanding the distribution and impact of these defects. The simulations

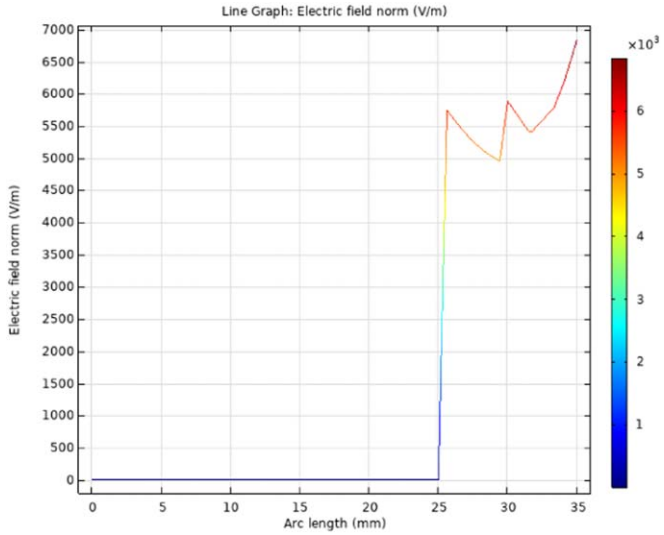


Figure 13. Electric field variation with respect to the radius of the cable end termination.

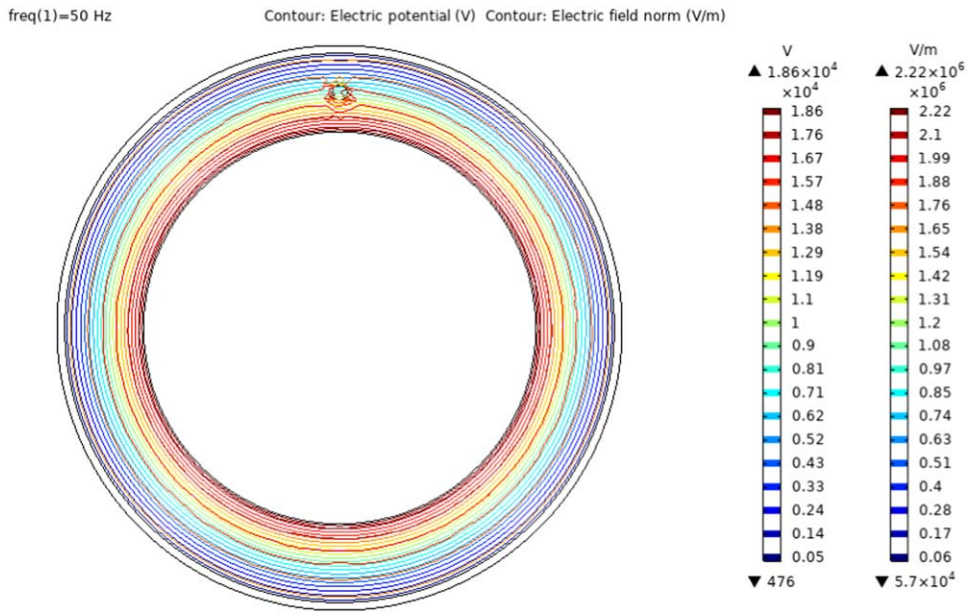


Figure 14. Electric field and potential distribution in a cable with air void of 1 mm diameter.

demonstrate how the electric potential and field are affected when air voids or pinhole cavities are positioned at various distances from the cable junction.

4.2.1. Spherical air voids

The potential and electric field distributions are simulated when a cable has several air-filled cavities. A simulated 1 mm-diameter air-filled cavity is seen in figure 7. Figure 14 illustrates the pronounced impact of a 1 mm air void on the electric field and potential distribution within the cable. The presence of the void induces a significant concentration of electric field at its periphery, resulting in elevated electrical stress. This localized stress intensification can predispose the cable to insulation breakdown, partial discharge activity, and accelerated aging, ultimately compromising the cable's overall reliability and lifespan. Figure 15 illustrates the spatial variation of the electric field along the cable's arc length, revealing pronounced peaks associated with the 1 mm air void. These electric field hotspots indicate regions of heightened electrical stress, which can significantly accelerate insulation degradation and predispose the cable to premature failure due to partial discharge and breakdown.

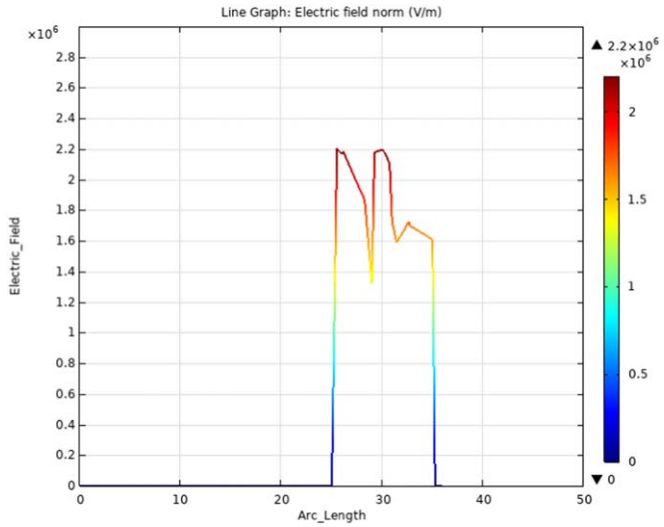
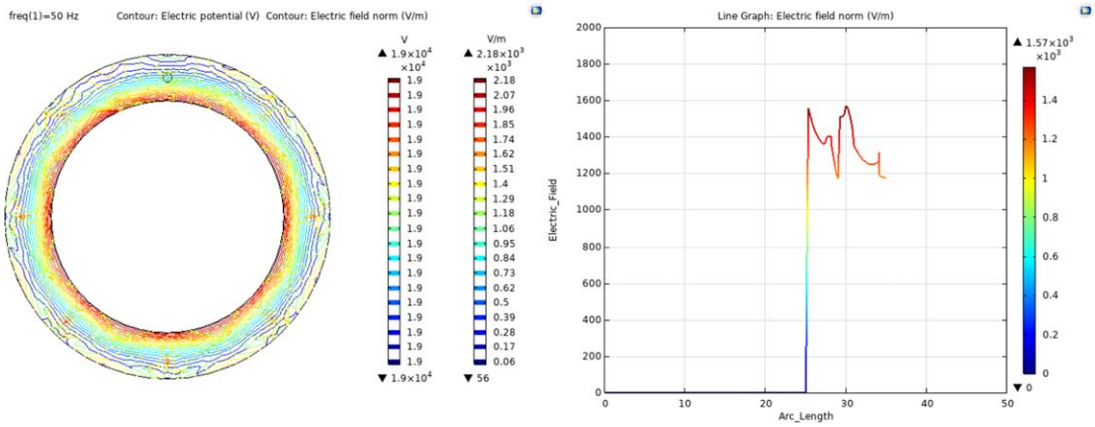


Figure 15. Changes in the electric field in a cable with air void of 1 mm diameter.

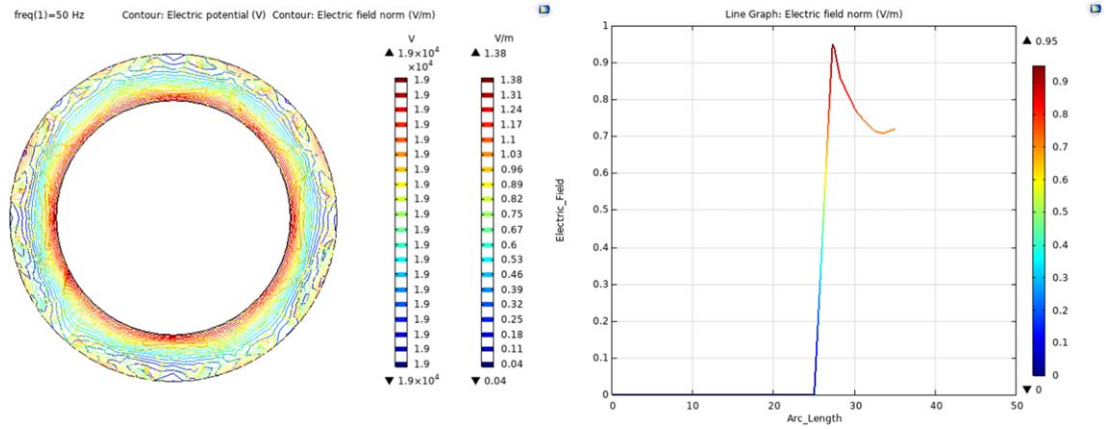


a. Electric field and potential distribution b. Variation of electric field

Figure 16. Inside the cable end termination with air void of 1 mm diameter at 100 mm distance from cable junction.

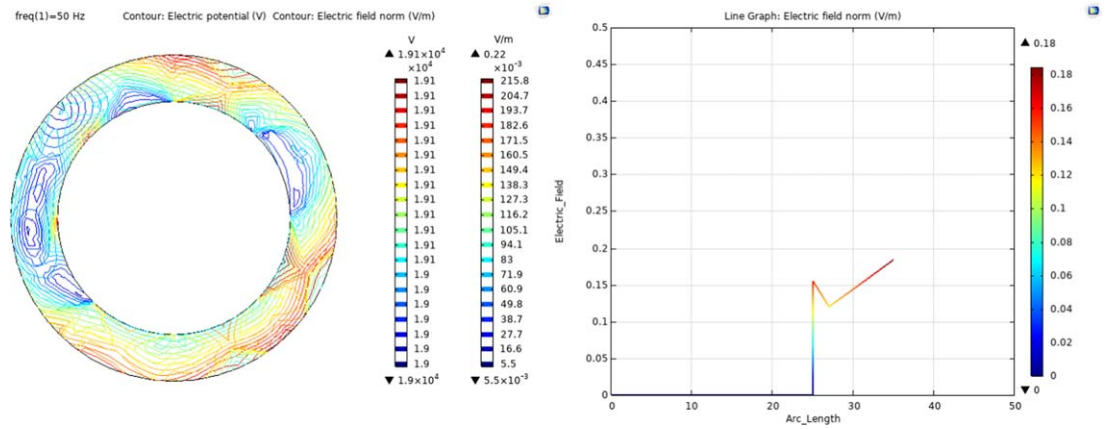
In order to have a comparative study between the cable and cable end termination, air filled cavity is simulated in cable end termination. It simulates how electric potential and electric field are distributed when an air void is positioned at a different location from the cable connection. Figure 16 illustrates the complex electric field and potential distribution within a cable end termination containing a 1 mm diameter air void 100 mm from the cable junction. The contour plot reveals a pronounced concentration of electric field around the air void, indicative of heightened electrical stress. The corresponding line graph emphasizes the non-uniform electric field distribution along the arc length, with distinct peaks correlating to regions of maximum stress. These findings underscore the critical role of air voids in exacerbating electrical stress within cable terminations, potentially leading to premature insulation failure.

The potential and electric field distributions are simulated in the presence of several kinds of air-filled cavities, as shown in figures 18–25. One mm of air space is situated 150 mm from the cable intersection. Figure 17 illustrate the electric field and potential distribution within a cable end termination featuring a 1 mm diameter air void positioned 150 mm from the cable junction. The contour plot in figure 17(a) reveals a complex interplay of electric potential and field intensity, with a pronounced concentration of electric field around the air void. This observation is corroborated by the line graph in figure 17(b), which depicts the variation of electric field along the arc length. The presence of multiple peaks in the electric field profile further emphasizes the non-uniform stress distribution within the termination, highlighting the critical influence of air voids on the overall electrical performance and potential failure modes of the cable system. Figure 18 present the electric field and potential distribution within a cable end termination featuring a 1 mm diameter air void situated 200 mm from



a. Electric field and potential distribution b. Variation of electric field

Figure 17. Inside the cable end termination with air void of 1 mm diameter at 150 mm distance from cable junction.



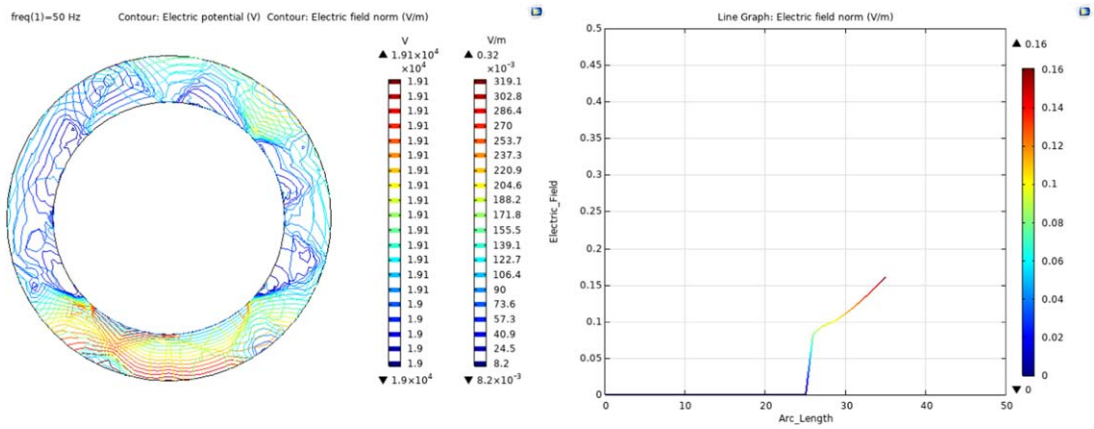
a. Electric field and potential distribution b. Variation of electric field

Figure 18. Inside the cable end termination with air void of 1 mm diameter at 200 mm distance from cable junction.

the cable junction. The contour plot in figure 18(a) illustrates the spatial variation of electric potential and field intensity, revealing a pronounced concentration of electric field around the air void. The corresponding line graph in figure 18(b) depicts the electric field distribution along the arc length, characterized by a distinct peak coinciding with the location of the air void. These findings underscore the persistent influence of air voids on the electric field distribution within cable terminations, even at increased distances from the cable junction, emphasizing the critical need for rigorous quality control and inspection procedures to mitigate potential failure risks.

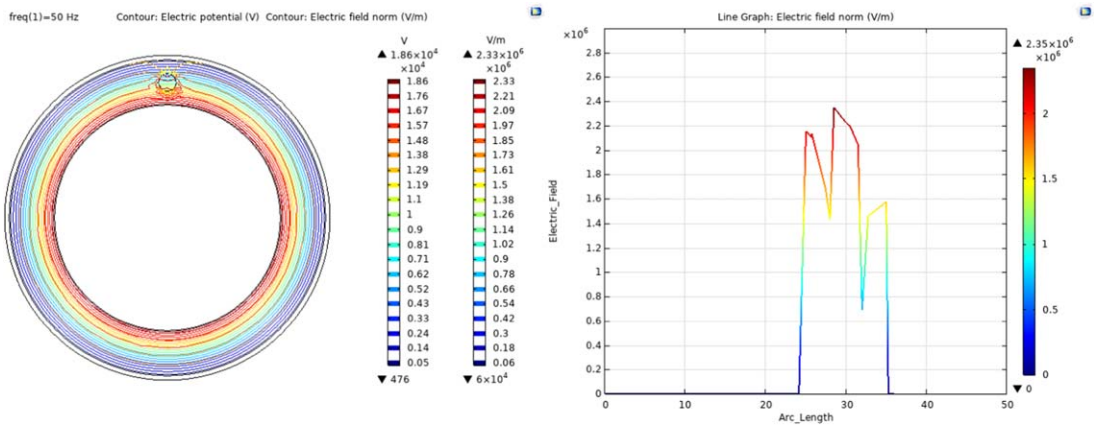
Figure 19 illustrate the electric field and potential distribution within a cable end termination featuring a 1 mm diameter air void situated 250 mm from the cable junction. The contour plot in figure 19(a) reveals a complex interplay of electric potential and field intensity, with a notable concentration of electric field around the air void. The corresponding line graph in figure 19(b) depicts the electric field distribution along the arc length, characterized by a distinct peak coinciding with the location of the air void. While the influence of the air void on the electric field distribution appears to diminish with increasing distance from the cable junction, the presence of significant field enhancements in the termination region underscores the potential for localized insulation stress and subsequent failure.

The distributions of the potential and electric fields are simulated when different types of air-filled cavities are present inside cables and cable junctions. A 2 mm air void is inserted inside each cable and cable junction. Figure 20 illustrate the electric field and potential distribution within a cable featuring a 2 mm diameter air void. The contour plot in figure 20(a) reveals a pronounced distortion of the electric field and potential patterns due to the presence of the air void. A significant concentration of electric field is observed around the void, indicative of



a. Electric field and potential distribution b. Variation of electric field

Figure 19. Inside the cable end termination with air void of 1 mm diameter at 250 mm distance from cable junction.

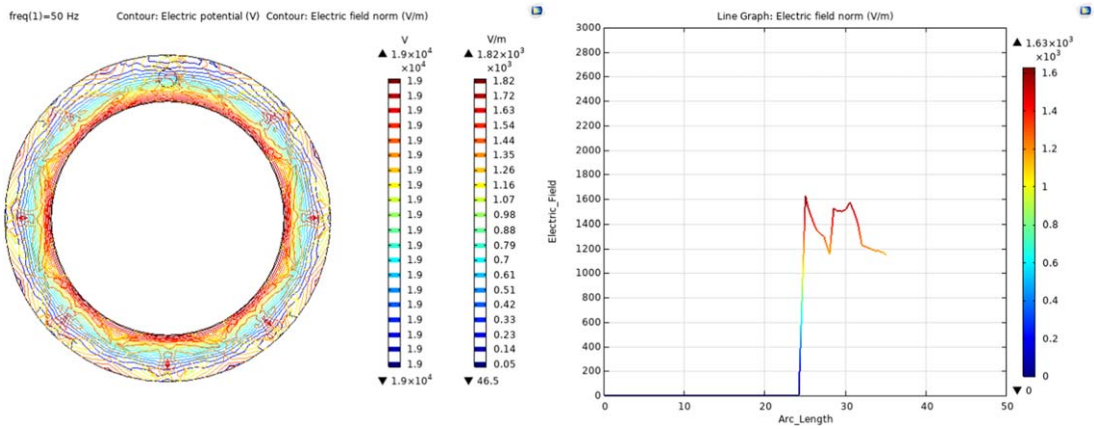


a. Electric field and potential distribution b. Variation of electric field

Figure 20. Inside the cable with air void of 2 mm diameter.

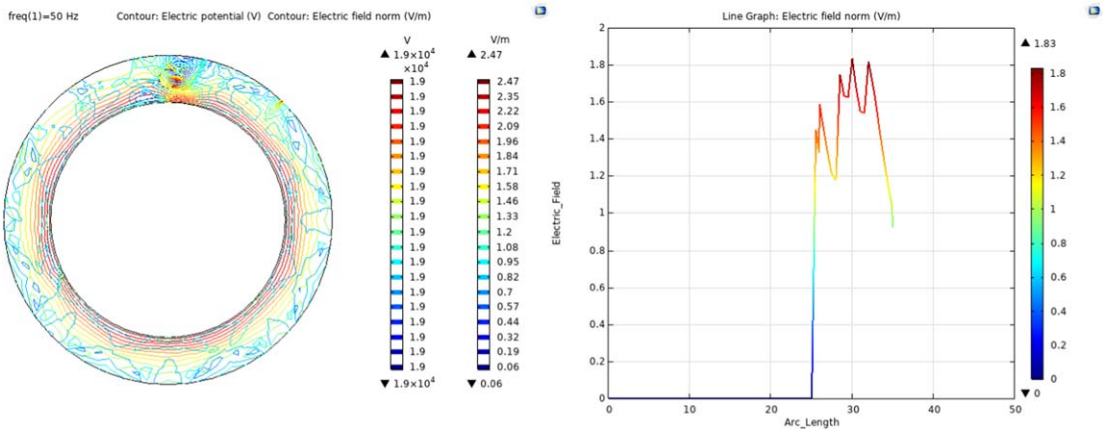
heightened electrical stress. The corresponding line graph in figure 20(b) depicts the electric field variation along the cable's arc length, emphasizing the non-uniform field distribution and the presence of sharp peaks associated with the air void. These findings underscore the critical impact of air void size on the electrical stress within cables, with larger voids leading to more pronounced field distortions and an increased risk of insulation failure. Figure 21 illustrate the electric field and potential distribution within a cable end termination featuring a 2 mm diameter air void situated 100 mm from the cable junction. The contour plot in figure 21(a) reveals a pronounced distortion of the electric field and potential patterns due to the presence of the larger air void compared to previous analyses. A significant concentration of electric field is observed around the void, indicative of heightened electrical stress. The corresponding line graph in figure 21(b) depicts the electric field variation along the cable's arc length, emphasizing the non-uniform field distribution and the presence of sharp peaks associated with the air void. These findings underscore the critical impact of air void size on the electrical stress within cables, with larger voids leading to more pronounced field distortions and an increased risk of insulation failure.

Figure 22 illustrates the electric field and potential distribution within a cable end termination featuring a 2 mm diameter air void positioned 150 mm from the cable junction. The contour plot in figure 22(a) reveals a pronounced distortion of the electric field and potential patterns due to the presence of the larger air void. A significant concentration of electric field is observed around the void, indicative of heightened electrical stress. The corresponding line graph in figure 22(b) depicts the electric field variation along the cable's arc length, emphasizing the non-uniform field distribution and the presence of sharp peaks associated with the air void. These findings underscore the critical impact of air void size and location on the electrical stress within cables, with larger voids and closer proximity to the termination leading to more pronounced field distortions and an



a. Electric field and potential distribution b. Variation of electric field

Figure 21. Inside the cable end termination with air void of 2 mm diameter at 100 mm distance from cable junction.

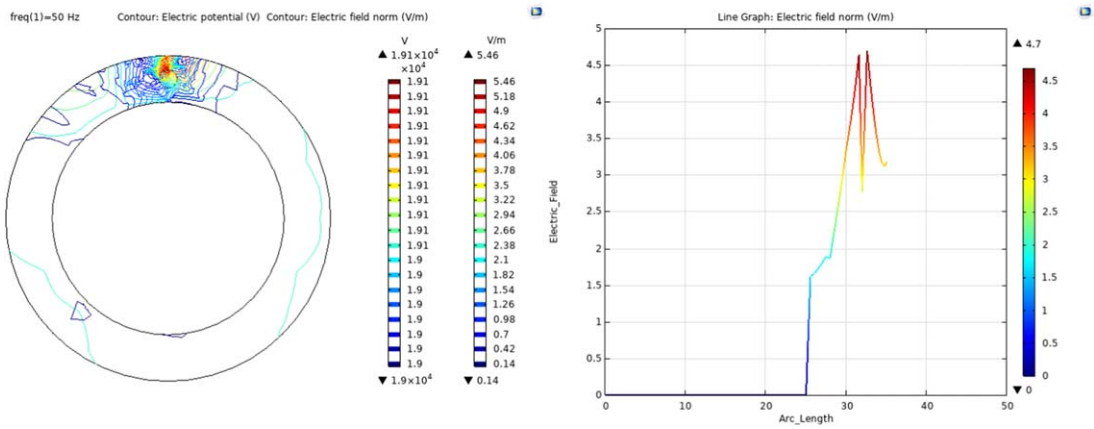


a. Electric field and potential distribution b. Variation of electric field

Figure 22. Inside the cable end termination with air void of 2 mm diameter at 150 mm distance from cable junction.

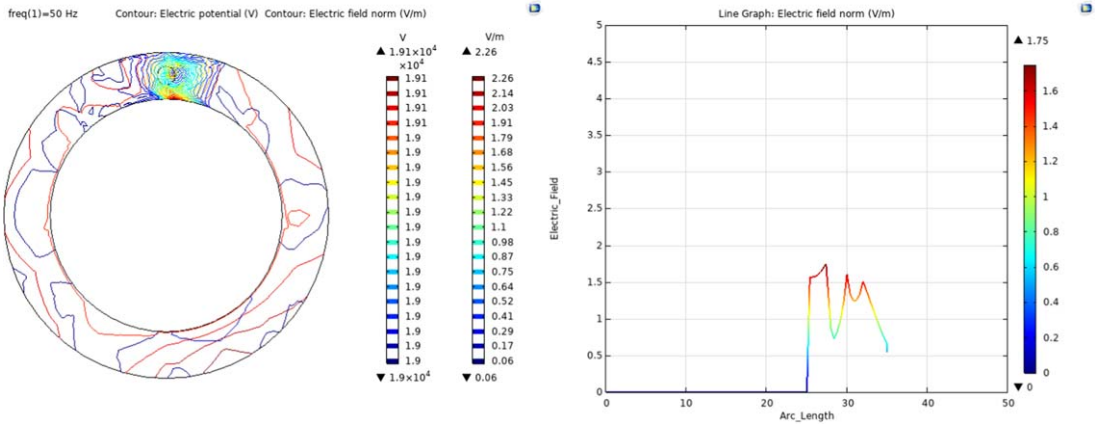
increased risk of insulation failure. Figure 23 illustrates the electric field and potential distribution within a cable end termination featuring a 2 mm diameter air void positioned 200 mm from the cable junction. The contour plot in figure 23(a) reveals a pronounced distortion of the electric field and potential patterns due to the presence of the larger air void. A significant concentration of electric field is observed around the void, indicative of heightened electrical stress. The corresponding line graph in figure 23(b) depicts the electric field variation along the cable's arc length, emphasizing the non-uniform field distribution and the presence of sharp peaks associated with the air void. These findings underscore the critical impact of air void size and location on the electrical stress within cables, with larger voids and closer proximity to the termination leading to more pronounced field distortions and an increased risk of insulation failure. Figure 24 illustrates the electric field and potential distribution within a cable end termination featuring a 2 mm diameter air void positioned 250 mm from the cable junction. The contour plot in figure 24(a) reveals a complex interplay of electric potential and field intensity, with a notable concentration of electric field around the air void. The corresponding line graph in figure 24(b) depicts the electric field variation along the arc length, characterized by multiple peaks and valleys. While the influence of the air void on the electric field distribution appears to diminish with increasing distance from the cable junction, the presence of significant field enhancements in the termination region underscores the potential for localized insulation stress and subsequent failure, necessitating further investigation into the long-term implications of such defects.

The potential and electric field distributions within the cable and cable end termination are simulated by placing a 1 mm and 2 mm diameter air void closer to the conductor. Figures 24–27 show the variation in potential and electric field distributions.



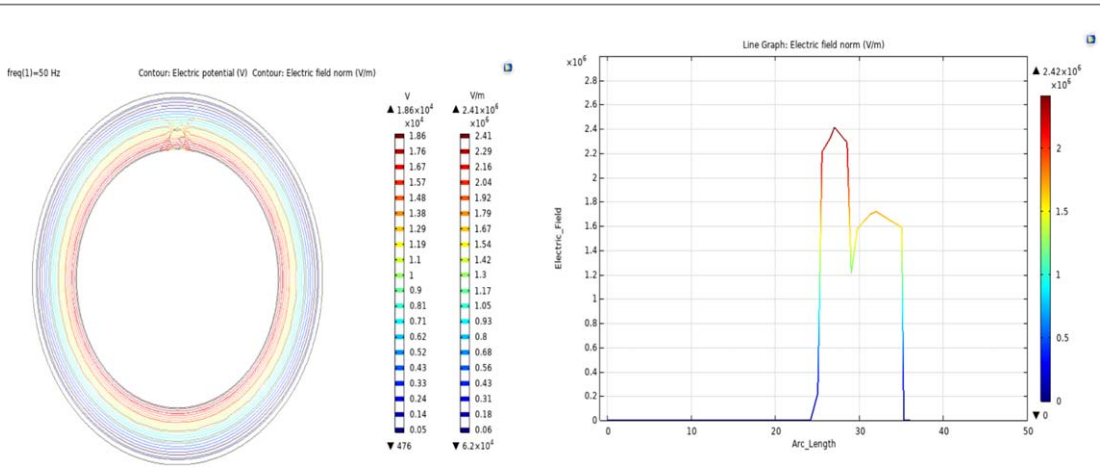
a. Electric field and potential distribution b. Variation of electric field

Figure 23. Inside the cable end termination with air void of 2 mm diameter at 200 mm distance from cable junction.



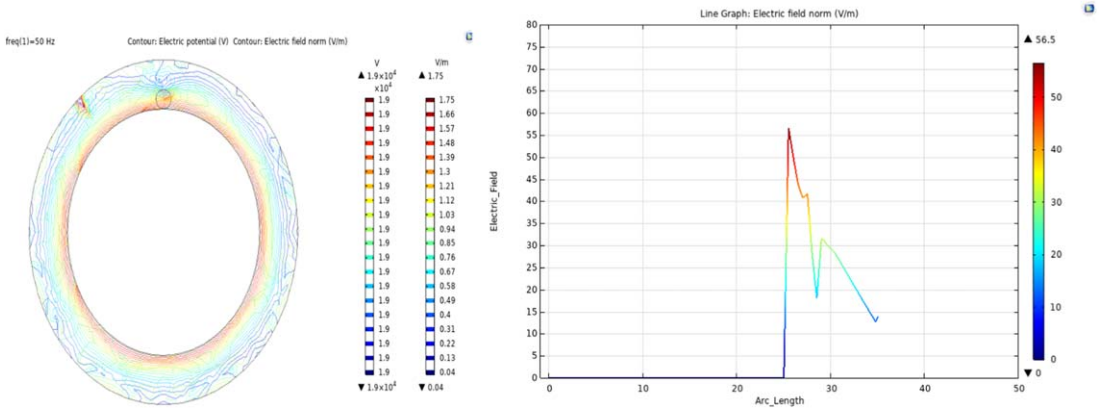
a. Electric field and potential distribution b. Variation of electric field

Figure 24. Inside the cable end termination with air void of 2 mm diameter at 250 mm distance from cable junction.



a. Electric field and potential distribution b. Variation of electric field

Figure 25. Inside the cable with air void of 1 mm diameter nearer to conductor.



a. Electric field and potential distribution b. Variation of electric field

Figure 26. Inside the cable end termination with air void of 1 mm diameter nearer to conductor.

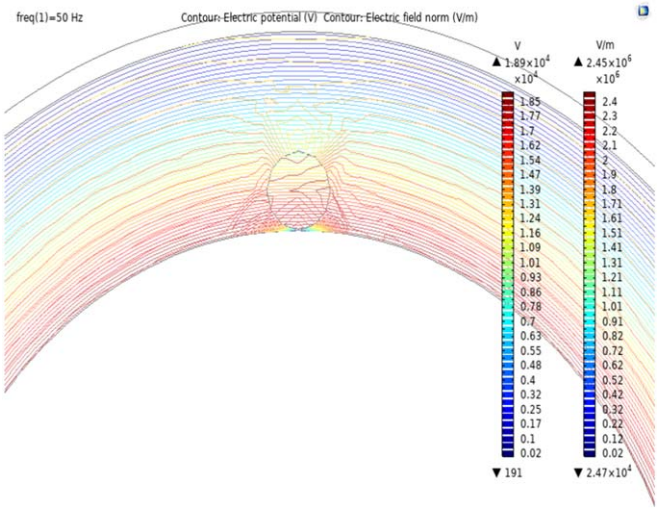


Figure 27. Electric field distortion inside cable with air void of 2 mm diameter nearer to conductor.

Since insulation has a higher dielectric strength ($\varepsilon_{r,Insulation}$) than air ($\varepsilon_{r,air}$), the following can be determined using the principle of electric displacement conservation:

$$\varepsilon_{r,air} \cdot E_{air} = \varepsilon_{r,Insulation} \cdot E_{Insulation} \quad (6a)$$

Thus, the ratio '$\varepsilon_{r,Insulation}/\varepsilon_{r,air}$' in'reases the electric field in the air, $\varepsilon_{r,air}$. When the cable is under voltage, at the air void cavity, and the ionization phenomena occurs in this void due to conduction current, which has available free electrons.

Thus, the ratio '$\frac{\varepsilon_{r,Insulation}}{\varepsilon_{r,air}}$' increases the 'lectric field in the air, E_{air}. While the cable is under voltage, at the air void cavity, and the ionization event occur in this void due to conduction current, which has available free electrons.

Figure 25 presents a comprehensive analysis of the electric field and potential distribution within a cable featuring a 1 mm diameter air void positioned closer to the conductor. The contour plot in figure 25(a) reveals a pronounced distortion of the electric field and potential patterns due to the presence of the air void. A significant concentration of electric field is observed around the void, indicative of heightened electrical stress. The contours of both electric potential and field strength exhibit a non-uniform distribution, deviating from the expected circular pattern in a defect-free cable. Figure 25(b) illustrates the variation of the electric field along the cable's arc length, characterized by pronounced peaks and valleys. These fluctuations in electric field intensity are directly attributed to the presence of the air void and its proximity to the conductor. The sharp increase in electric field magnitude near the air void highlights the potential for localized stress concentration and subsequent insulation breakdown. Figure 26 presents a comprehensive analysis of the electric field and potential

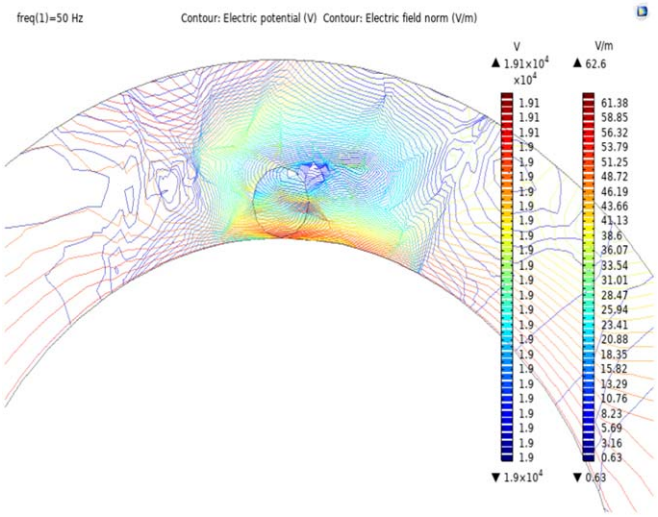


Figure 28. Electric field distortion inside cable end termination with air void of 2 mm diameter nearer to conductor.

distribution within a cable end termination featuring a 1 mm diameter air void positioned closer to the conductor. Figure 26(a) illustrates the electric field and potential distribution within the cable end termination. The contour plot vividly depicts the distortion of the electric field and potential patterns due to the presence of the air void. A pronounced concentration of electric field is observed around the void, forming a distinct 'hotspot', indicative of heightened electrical stress. The contours of both electric potential and field strength exhibit a non-uniform distribution, deviating significantly from the expected circular pattern in a defect-free cable. Figure 26(b) depicts the variation of the electric field along the cable's arc length. The line graph presents a non-uniform electric field distribution, characterized by pronounced peaks and valleys. These fluctuations in electric field intensity are directly attributed to the presence of the air void and its proximity to the conductor. The sharp increase in electric field magnitude near the air void, reaching a peak of approximately 56.5 V/m, highlights the potential for localized stress concentration and subsequent insulation breakdown.

Figure 27 depicts the electric field distortion within a cable containing a 2 mm diameter air void positioned closer to the conductor. The contour plot reveals a pronounced intensification of the electric field around the air void, forming a distinct 'hotspot'. This region of high electric stress is visually evident through the concentrated and closely spaced electric field norm contours. The overall electric field pattern is significantly distorted compared to a defect-free cable, with the field lines exhibiting a non-uniform and curved distribution. Figure 28 illustrates the electric field distortion within a cable end termination containing a 2 mm diameter air void positioned closer to the conductor. The contour plot vividly depicts a pronounced intensification of the electric field around the air void, forming a distinct 'hotspot'. This region of heightened electrical stress is visually evident through the concentrated and closely spaced electric field norm contours. The overall electric field pattern is significantly distorted compared to a defect-free cable, with the field lines exhibiting a non-uniform and curved distribution.

The distribution of the electric field changes from cable to cable end termination, as shown in figures 15, 16, 20, and 21, and the electric field's intensity is higher in areas where there is a void in the cable than at the cable end termination. A 1 mm diameter air void inside the cable at 2.2×10^{-6} (V/m) shown in figures 13 and (a) cable end termination at 1.57×10^{3} (V/m) shown in figure 15 as well as a 2 mm diameter air void inside the cable at 2.35×10^{6} (V/m) shown in figures 18(a) and (a) cable end termination at 1.63×10^{3} (V/m) shown in figure 20 from the cable junction indicate the variability of maximum electric field intensity.

From figures 16–19, the maximum of electric field distribution within the cable end termination with air void of 1 mm diameter at distances of 100 mm, 150 mm, 200 mm and 250 mm from cable junctions are 1.57 kV mm^{-1}, 0.9 kV mm^{-1}, 0.18 V mm^{-1} and 0.16 V mm^{-1}, respectively. It can also be seen that when the void moves away from the cable, the intensity of the electric field decreases from 1.57×10^{3} (V/mm) to 0.16 (V/mm), as seen in figures 16–19.

And also from the figures 21–24, the maximum of electric field distribution within the cable end termination with air void of 2 mm diameter at distances of 100 mm, 150 mm, 200 mm and 250 mm from cable junctions are 1.63 kV mm^{-1}, 4.7 V /m m , 1.83 V mm^{-1} and 1.75 V mm^{-1}, respectively. It can also be seen that when the void moves away from the cable, the intensity of the electric field decreases from 1.63×10^{3} (V/mm) to 1.75 (V/mm), as seen in figures 21–24.

Table 3. Electric field intensity with a 1 mm and 2 mm diameter air void.

Sl. no.	Particular	Electric field (V/mm)	
		1 mm	2 mm
1.	Inside the cable	2.2×10^6	2.35×10^6
2.	Cable end termination	1.57×10^3	1.63×10^3

Table 4. Electric field intensity with a 1 mm and 2 mm diameter air void at cable end termination.

Sl. no.	Distances (mm)	Electric field (V/mm)	
		1 mm	2 mm
1.	100	1.57 K	1.63 K
2.	150	0.9 K	4.7
3.	200	0.18	1.83
4.	250	0.16	1.75

Table 5. Electric field intensity with a 1 mm and 2 mm diameter air void nearer to the conductor.

Sl. no.	Particular	Electric field (V/mm)	
		1 mm	2 mm
1.	Inside the cable	2.42×10^6	2.45×10^6
2.	Cable end termination	56	62.6

To conduct a comparative study, tables 3–5 show the electrified variation with air void existence at various diameters and positions near to the conductor in the cable to cable-to-cable end termination.

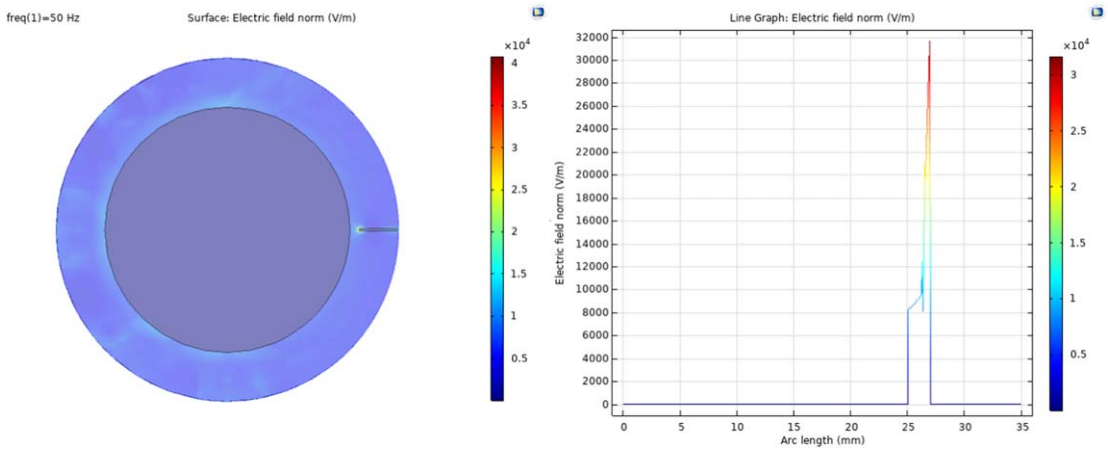
Table 3 demonstrates that increasing the diameter of air voids near the cable junctions leads to higher electric fields, with varying electric field distributions from the cable to the cable end termination. Table 4 indicates that increasing the diameter of air voids near the cable junctions results in higher electric fields, while the electric field distribution within the cable end termination decreases at different locations. Table 5 shows that increasing the diameter of air voids closer to the conductor leads to higher electric fields, with varying electric field distributions from the cable to the cable end termination.

Furthermore, the presence of an air void with a diameter of 1 mm nearer to the conductor causes the electric field distribution to differ from cable to cable end termination. Inside the cable displayed in figure 26 has a higher electric field intensity (2.42×10^6 V mm^{-1}) compared to the cable end termination indicated in figure 27, which has an electric field intensity of 56.5 V mm^{-1}. The cable shown in figure 28 has a larger electric field intensity (2.45×10^6 V mm^{-1}) than the cable end termination shown in figure 29, which has an electric field intensity of 62.6 V mm^{-1} with an air void of 2 mm diameter closer to the conductor.

Based on the observations made above, it is possible that if voids exist closer to the cable junction, the electric field intensity and distortion will be larger, resulting in cable end termination failure. A void closer to the cable junction leads the cable end termination to fail sooner than a void farther away.

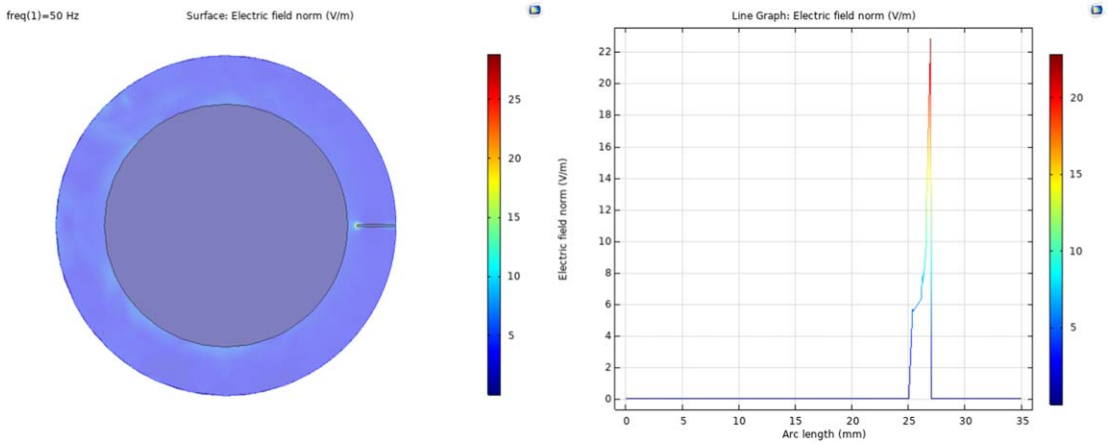
4.2.2. Pin hole

Cavity filled with a pinhole with a radius of 0.1 mm and a height of 8 mm as shown in figure 8 is simulated. The small pinhole may appear during the installation of the cable end kit as a result of faulty assembly. The electric field distributions are simulated in the case of a pinhole. A pinhole with a radius of 1 mm and a height of 8 mm is put at 100 mm, 150 mm, and 200 mm from the cable junction. Figure 29 illustrates the electric field distribution within a cable end termination containing a pinhole defect with a radius of 0.1 mm and a height of 8 mm, located 100 mm from the cable junction. Figure 29(a) depicts the electric field distribution across the cable cross-section, revealing a pronounced concentration of electric field around the pinhole, indicative of a localized region of heightened electrical stress. The field lines exhibit a distorted pattern, converging towards the pinhole and diverging outwards, suggesting a significant impact on the entire electric field profile. Figure 29(b) presents



a. Distribution of electric field within the cable end termination b. Variation of electric field

Figure 29. Inside the cable end termination with pin hole of radius 0.1 mm and height 8 mm at 100 mm from the cable junction.

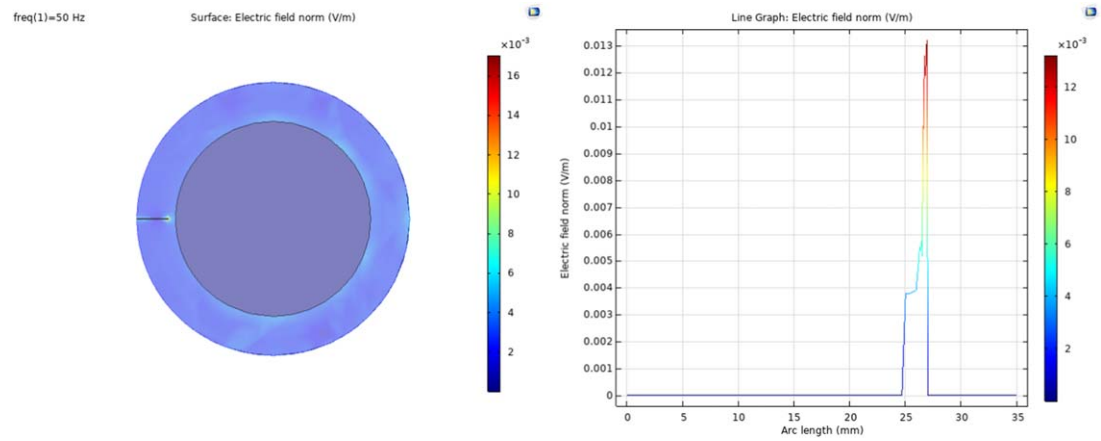


a. Distribution of electric field within the cable end termination b. Variation of electric field

Figure 30. Inside the cable end termination with pin hole of radius 0.1 mm and height 8 mm at 150 mm from the cable junction.

the electric field variation along the cable's arc length, demonstrating a sharp peak coinciding with the location of the pinhole. This localized electric field enhancement underscores the critical role of pinhole defects in exacerbating electrical stress within cable terminations, potentially leading to premature insulation breakdown and system failure. Figure 30 illustrates the electric field distribution within a cable end termination containing a pinhole defect with a radius of 0.1 mm and a height of 8 mm, located 150 mm from the cable junction. Figure 30(a) depicts the electric field distribution across the cable cross-section, revealing a pronounced concentration of electric field around the pinhole, indicative of a localized region of heightened electrical stress. The field lines exhibit a distorted pattern, converging towards the pinhole and diverging outwards, suggesting a substantial effect on the overall electric field profile. Figure 30(b) presents the electric field variation along the cable's arc length, demonstrating a sharp peak coinciding with the location of the pinhole. This localized electric field enhancement underscores the critical role of pinhole defects in exacerbating electrical stress within cable terminations, potentially leading to premature insulation breakdown and system failure.

Figure 31 illustrates the electric field distribution within a cable end termination containing a pinhole defect with a radius of 0.1 mm and a height of 8 mm, located 200 mm from the cable junction. Figure 31(a) depicts the electric field distribution across the cable cross-section, revealing a pronounced concentration of electric field around the pinhole, indicative of a localized region of heightened electrical stress. The field lines exhibit a distorted pattern, converging towards the pinhole and diverging outwards, suggesting a substantial effect on the overall electric field profile. Figure 31(b) presents the electric field variation along the cable's arc length, demonstrating a sharp peak coinciding with the location of the pinhole. This localized electric field



a. Distribution of electric field within the cable end termination b. Variation of electric field

Figure 31. Inside the cable end termination with pin hole of radius 0.1 mm and height 8 mm at 200 mm from the cable junction.

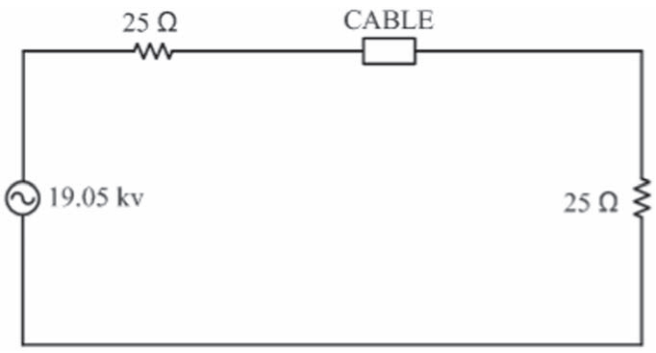
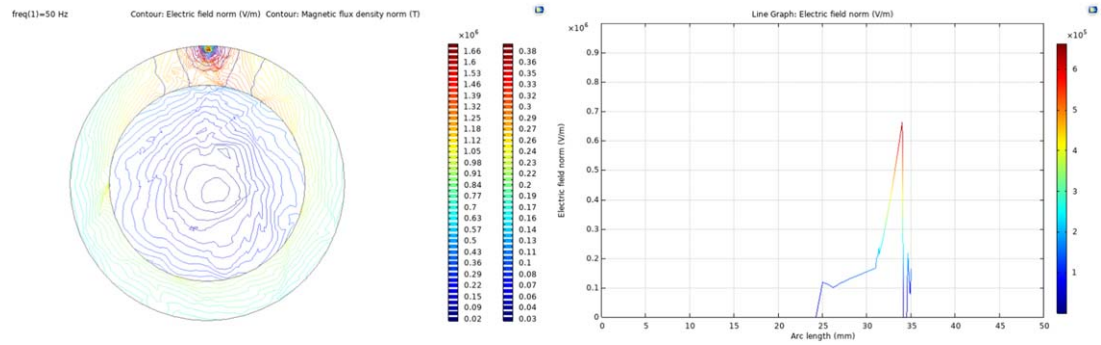


Figure 32. Electromagnetic field simulation circuits.

enhancement underscores the critical role of pinhole defects in exacerbating electrical stress within cable terminations, potentially leading to premature insulation breakdown and system failure. The pinhole cavity in the cable end termination is simulated in order to conduct a study there. The electric field's distribution with a pinhole placed at different locations from the cable junction is simulated. As illustrated in figures 29–31, the electric field intensity drops from 32 kV mm^{-1} to 0.0125 kV mm^{-1} as the pinhole moves away from the cable joints. As a result, if a pinhole occurs at the cable junction during the installation process, the electric field intensity and distortion will be increased, resulting in cable end termination failure. A pinhole at the cable junction causes the cable end termination to fail prematurely. Under normal operating conditions, the high electric field deformations around XLPE insulation defects are relatively acute, and they have a detrimental impact on insulation breakdown. The insulation breaks as a result of the mechanical strains created by these cavities.

4.3. Electromagnetic field simulation

Figure 32 depicts the electromagnetic field circuit as simulated in COMSOL software. The resistance rating is modified so that the cable is subjected to the specified single phase to ground voltage (19.05 kV) and rated current of 400 amps. The current flowing through the cable is around 366 amps. This circuit simulates a practical real-time scenario where the cable load current approaches its full load carrying capacity, and the applied voltage is the rated single-phase voltage.



a. Electric field and Magnetic field b. Variation of electric field

Figure 33. Inside the cable end termination with partial semiconducting layer on the top of XLPE insulation.

4.3.1. Partial semiconducting layer on top of XLPE insulation

During the cable end kit installation process, there is a possibility that remnants of the semiconducting layer may remain on the XLPE insulation. The electric and magnetic field distributions under these conditions are simulated, with a detailed mesh diagram provided in figure 9. Figure 33 illustrates the electric and magnetic field distributions within a cable end termination featuring a partial semiconducting layer atop the XLPE insulation. Figure 33(a) presents a contour plot depicting the electric field norm and magnetic flux density norm. The contour lines reveal a non-uniform distribution of both fields, with a concentration of electric field in specific regions. Figure 33(b) provides a line graph showcasing in the changes of electric field norm along the cable's arc length. The graph exhibits a complex pattern with multiple peaks and valleys, indicating significant fluctuations in electric field intensity. These observations highlight the impact of the partial semiconducting layer on the electromagnetic field distribution within the cable termination, which may have implications for insulation performance and overall cable reliability.

4.3.2. Electric and magnetic field simulation for pinhole

During the cable installation procedure, there is a possibility of a puncture at the cable end kit, as well as small pin holes caused by faulty assembly, which simulate the electric and magnetic field distributions.

Figure 34 presents a contour plot illustrating the distribution of electric field norm and magnetic flux density norm within a cable end termination. The image reveals a complex interplay between the electric and magnetic fields, with both exhibiting non-uniform patterns. The electric field is concentrated in specific regions, suggesting areas of higher electrical stress. Similarly, the magnetic flux density demonstrates variations across the termination, indicating the presence of induced currents and associated magnetic fields. The interdependence of these fields is evident in the contour plot, highlighting the need for a comprehensive analysis of both electric and magnetic phenomena to fully understand the behavior of the cable end termination under operational conditions figure 35 illustrates the variation of electric and magnetic fields within a cable end termination. Figure 35(a) depicts the electric field norm along the cable's arc length, revealing a non-uniform distribution characterized by multiple peaks and valleys. The electric field intensity exhibits significant fluctuations, with localized regions of high field strength. Figure 35(b) presents the magnetic flux density norm, showcasing a similar non-uniform pattern with variations in intensity along the arc length. The correlation between the electric and magnetic field profiles suggests a complex electromagnetic interaction within the termination. These findings underscore the importance of considering both electric and magnetic fields for a comprehensive understanding of cable performance and potential failure mechanisms.

Table 6 compares electric field intensity values for spherical defects across different materials, presenting data from various studies alongside the proposed method. At the Near Conductor Surface, the proposed method exhibits the lowest intensity of 1.4 kV mm^{-1}, out performing the values of 1.7 kV mm^{-1}, 1.8 kV mm^{-1}, and 2.1 kV mm^{-1} reported by [18, 19], and [20], respectively. This indicates superior insulation performance near the conductor, potentially reducing breakdown risks. For the Middle of Insulator, the proposed method's value of 1 kV/mm is lower than the 1.1 kV mm^{-1}, 1.3 kV mm^{-1}, and 1.4 kV mm^{-1} reported by [18, 19], and [20], suggesting enhanced stability and insulation effectiveness within the insulator bulk. Similarly, at the Near Insulator Surface, the proposed method shows the lowest electric field intensity of 0.7 kV mm^{-1}, compared to 0.9 kV mm^{-1}, 1.1 kV mm^{-1}, and 1.3 kV/mm from [18, 19], and [20], respectively, highlighting its effectiveness in minimizing surface breakdown risks. Overall, the proposed method demonstrates improved insulation performance across all measured locations compared to existing methods.

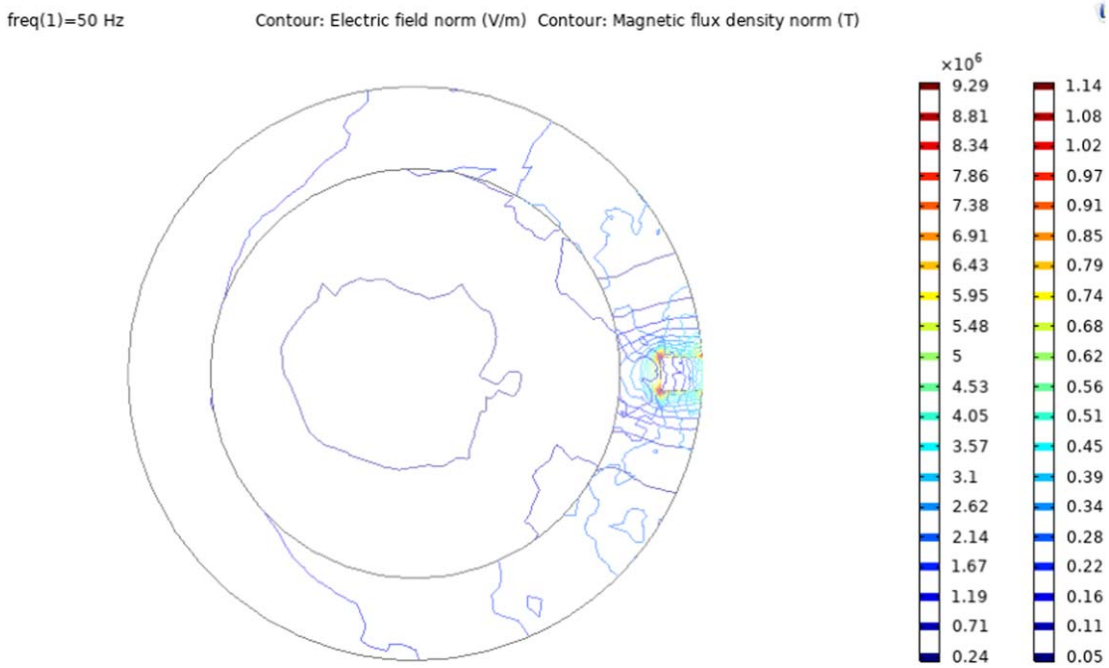


Figure 34. Magnetic fields and electric fields variation inside the cable end termination.

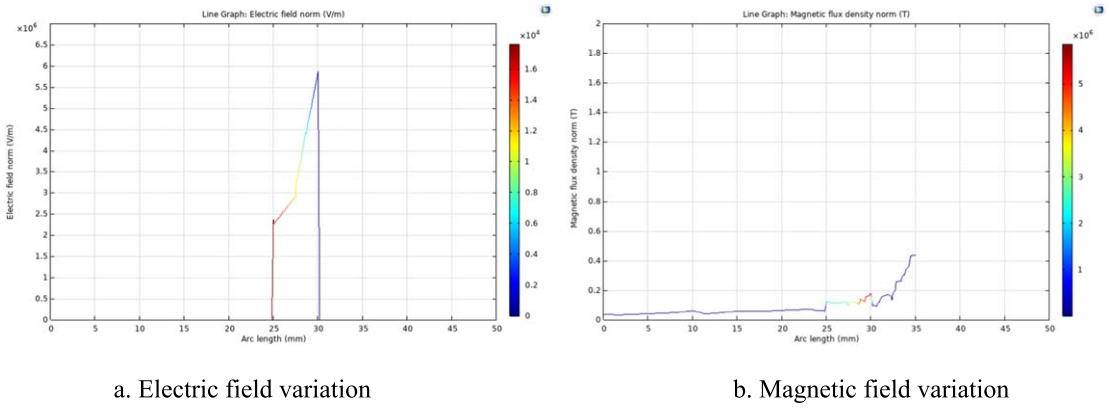


Figure 35. Electric fields and magnetic fields variation inside the cable end termination.

Table 6. Comparison of electric field intensity in spherical defect.

Study	Electric field intensity (kV/mm)		
	Near conductor surface	Middle of insulator	Near insulator surface
Proposed	1.4	1	0.7
[18]	1.7	1.1	0.9
[19]	1.8	1.3	1.1
[20]	2.1	1.4	1.3

Table 7 presents a comparison of magnetic field intensity values measured at 1 meter above the ground from various studies, including the proposed method. The proposed method demonstrates a magnetic field value of 206 μT, which is lower than the 211 μT reported by [18], 223 μT by [19], and 217 μT by [20]. This lower magnetic field value signifies that the proposed method achieves a reduction in magnetic field exposure, which is beneficial for minimizing potential health risks and reducing electromagnetic interference.

Table 7. Comparison of magnetic field at 1 m above the ground.

Study	Magnetic field (μT)
Proposed	206
[18]	211
[19]	223
[20]	217

4.4. Discussion

The simulation results obtained through COMSOL Multiphysics provide detailed insights into how cavities, such as spherical air voids and pinholes, affect the distribution of electric fields within cables and their terminations. Initially, simulations without cavities show a predictable pattern of electric field symmetry around the conductor, with the highest field strengths concentrated near the conductor and gradually diminishing towards the cable insulation ends. However, when cavities are introduced, this symmetry is disrupted. Spherical air voids and pinholes create localized regions of intensified electric fields, particularly near the cavities and within the cable end termination zones. These regions experience significantly higher electric field strengths compared to unaffected areas, indicating a heightened risk of insulation breakdown and potential failure at these critical points.This study represents a significant advancement by not only employing COMSOL Multiphysics for detailed simulations but also by integrating a comprehensive analysis of how different defects affect electric field distributions.The results reveal that larger cavities and those closer to the conductor result in more pronounced electric field variations. This finding emphasizes the need for precise installation practices and robust quality control to mitigate these risks.To bridge the gap between simulation results and practical engineering applications, several concrete measures are recommended. Enhanced detection techniques such as high-resolution x-ray tomography or ultrasonic testing should be implemented to accurately identify and quantify air voids and pinholes during cable manufacturing and installation. Quality control protocols need to be developed and enforced to ensure adherence to design specifications, including regular inspections and maintenance to address potential defects before they impact system reliability. Design modifications should be considered to accommodate or mitigate defect impacts, such as redesigning stress control tubes and insulation materials to handle localized electric field intensifications. Additionally, establishing preventive maintenance programs based on the study's insights will help monitor electric field strengths and insulation conditions, identifying issues before they result in failures.These recommendations aim to translate simulation insights into practical solutions that can significantly improve the reliability and performance of underground power transmission systems. By integrating these measures, the industry can enhance its ability to manage and mitigate the effects of defects in cable systems, thereby reducing the risk of failures and extending the lifespan of critical infrastructure.

5. Conclusion

This study in COMSOL Multiphysics analyzes how spherical air voids, pinholes, and irregularities in semiconducting layers affect electric fields and potential distributions in XLPE-insulated cable end terminations for medium voltage power transmission. The simulations show significant electric field variations due to different defect types and sizes, pinpointing areas prone to stress concentration. The introduction of a detailed analysis and novel approach using COMSOL Multiphysics provides new insights into the behavior of XLPE-insulated cables under electromagnetic stress. These insights are crucial for optimizing cable design and installation practices, aiming to enhance power transmission reliability. By examining electromagnetic stress effects, this research guides mitigating aging and installation-related failures in cable terminations. The simulation results reveal that the presence of air voids and pinholes induces varied electric field strengths within cables and terminations. Electric field intensities range prominently, such as 2.45×10^6 V/mm near the conductor and 56.5 V mm^{-1} at the cable end termination for 2 mm diameter voids, and 2.2×10^6 V mm^{-1} inside the cable and 1.57×10^3 V mm^{-1} at the termination for 1 mm voids. These findings underscore the critical influence of cavity characteristics on insulation integrity and potential failure risks in cable systems under operational loads. In light of these findings, the study advocates for specific engineering practices, including enhanced diagnostic techniques, rigorous quality control protocols, and design modifications to address the identified defects. Implementing these recommendations can lead to improved reliability and reduced downtime in power transmission networks. Future research should focus on refining these approaches and exploring additional factors that may influence cable performance. This research not only advances our understanding of cable behavior under operational stresses but also provides actionable insights to enhance the

durability and reliability of medium voltage power transmission systems. The integration of simulation results into practical industry practices is expected to contribute significantly to the advancement of cable technology and infrastructure resilience.

Data availability statement

All data that support the findings of this study are included within the article (and any supplementary files).

ORCID iDs

Suresh Haleyur Lakshmegowda https://orcid.org/0000-0002-6269-3274
Mahipal Bukya https://orcid.org/0000-0002-2507-7501

References

[1] Angadi M R V 2023 Introduction to under ground cabling *Electrical Engineering Concepts and Applications* **16**
[2] Benguesmia H, Seghiri H, Akka A R, Khadar S and M'ziou N 2020 Numerical study of electrical field distribution in insulation function of HV cables containing cavities using comsolmultiphysics *9ème Journées des sciences de l'ingénieur JSI* **2020**
[3] Benguesmia H, Seghiri A A R, Khadar H and M'ziouN S 2020 Study of a partial discharge in an HV cable usingfinite element method *9ème Journées des sciences del'ingénieur JSI* **2020**
[4] Arikan O, Uydur C C and Kumru C F 2023 Insulation evaluation of MV underground cable with partial discharge and dielectric dissipation factor measurements *Electr. Power Syst. Res.* **220** 109338
[5] Liu Z, Cui X, Li X, Zhan Y and Zhao Z 2023 Interface finite volume method with low calculating amount for step size varying electro-quasistatic field problem *CSEE Journal of Power and Energy Systems* **9** 2280–8
[6] Bukya M and Kumar R 2020 Safety consideration and design of high voltage cable for electric vehicle *2020 international conference on power electronics & IoT applications in renewable energy and its control (PARC)* (IEEE) 485–90
[7] Nadolny Z 2022 Electric field distribution and dielectric losses in XLPE insulation and semiconductor screens of high-voltage cables *Energies* **15** 4692
[8] Pietrzak P P 2023 Development of tests and methods of analysis for multi-factor ageing, degradation monitoring and/or lifetime modelling of an electrical insulation system of electrical motors (used in electric vehicle) *Doctoral dissertation, Institute National Polytechnique de Toulouse-INPT*
[9] Arati B 2023 *Manufacturing and characterization of self-healing polymer materials intended for the electrical insulation of future power modules (Doctoral dissertation, University Paul Sabatier-Toulouse III)*
[10] Bukya M, Kumar R and Mathur A 2023 Numerical investigation on thermal and electrical stress in electric vehicle cabling network *Journal of Advanced Research in Fluid Mechanics and Thermal Sciences* **102** 25–36
[11] Bukya M, Kumar R and Mathur A 2023 Analytical computation of thermal and electrical issues in E-mobility cabling network *Journal of Advanced Research in Fluid Mechanics and Thermal Sciences* **104** 84–92
[12] Gugulothu B N, Lakshminarayanan S, Palati M and Lakshmegowda S H 2023 A novel method to improve the residual life of switchgear by reducing the impact caused by thermal and mechanical stresses produced due to SLG cable faults in electrical substations *Journal of Advanced Research in Fluid Mechanics and Thermal Sciences* **106** 68–77
[13] Wang M, Liu Y, Huang Y, Xin Y, Han T and Du B 2024 Defect identification of XLPE power cable using harmonic visualized characteristics of grounding current *Electronics* **13** 1159
[14] Gao G, Zhou S, Yang S, Chen K, Xin D, Tang Y and Wu G 2023 Accurate identification partial discharge of cable termination for high-speed trains based on wavelet transform and convolutional neural network *Electr. Power Syst. Res.* **225** 109838
[15] Li X, Liu T, Sun W, Liang X, Wei Y, Hao C and Li G 2023 Influence and mechanism analysis of acid or alkali damp environment on insulation performance of distribution cable accessories *Eng. Fail. Anal.* **152** 107469
[16] Shingne N R, Dhiman G S, Puntambekar U N and Chetwani S H 2022 Analysis of failed cable termination: role of workmanship and electrical stresses *CIGRE, Session* (Electrical Research and Development Association (ERDA))
[17] van der Wielen P, He H, Maanen B, Pultrum E and Steennis F 2020 Statistics, experiences and learnings from failures in power cable systems during PQ and type tests, tests after installation and service operation *DNV GL, KEMA Labs (CESI) and Eindhoven University of Technology* 48 (CIGRE Sess) 1–12
[18] Arikan O and Kalenderli O 2021 The effect of insulation defects on electric and magnetic field distributions in power cables *Tehničkivjesnik* **28** 1152–60
[19] Florkowski M 2020 Influence of insulating material properties on partial discharges at dc voltage *Energies* **13** 4305
[20] Boudjella H, Ayad A N, Rouibah T, Larouci B, Alghamdi T A, Althobaiti A and Tayeb A S 2022 Magnetic field evaluation around 400 KV underground power cable under harmonics effects *Diagnostyka* **23**
[21] Bakri B, Benguesmia H, Mira A and M'ziou N 2023 Impact of heterogeneous cavities on the electrical constraints in the insulation of high-voltage cables *Diagnostyka* **24**
[22] Medoukali H and Zegnini B 2023 The impact of layout and concentration of defects on the electromechanical constraints in the MV cables insulation *Diagnostyka* **24**
[23] Elaggoune A, Seghier T, Zegnini B and Mohammed B 2021 Partial discharge activity diagnosis in electrical cable terminations using neural networks *Transactions on Electrical and Electronic Materials* **8** 19726–36
[24] Arabul A Y and Kumru C F 2023 Thermal analysis of xlpe insulated submarine cables for different loading conditions *Journal of Naval Sciences and Engineering* **19** 35–51
[25] COMSOL Group Ltd. 2016 Stockholm, Sweden*ComsolMultiphysics Software Package Version 5.2*
[26] Ghasemzadeh M R, Faghihi F and Mozafari S B 2023 FEM analysis of elliptical void in insulator of GIS compartment based on electric field distribution *Electr. Power Syst. Res.* **220** 109261

[27] Xia Z, Bhatti A A, Peng X, Yang B, Zhou H, Zhao C and Xie C 2020 Electric field and temperature distribution of high voltage cables with the addition of particles based on COMSOL simulation *2020 IEEE Int. Conf. on High Voltage Engineering and Application (ICHVE)* (IEEE) 1–4
[28] Da Silva M V, De Araújo O M, De Oliveira D F and Lopes R T 2024 Evaluation of the effects of voids in electrical cables using COMSOL multiphysics software *IEEE Trans. Dielectr. Electr. Insul.* **31** 2144–50
[29] Pugach V N, Polyakov D A, Nikitin K I, Zakharov I L and Petukhova N N 2019 Analysis of temperature conditions influence on cables insulation operation life *J. Phys. Conf. Ser.* 1260 (IOP Publishing) 052027
[30] Qin S, Xu Q, Wang Q, Zhang J, Ju Z, Hou Z and Zhang J 2022 Study on temperature rise characteristics of 110 kV XLPE cable under different service years considering dielectric loss *Energy Reports* **8** 493–501
[31] Zhao Y, Han Z, Xie Y, Fan X, Nie Y, Wang P and Zhu W 2020 Correlation between thermal parameters and morphology of cross-linked polyethylene *IEEE Access* **8** 19726–36
[32] Shahtaj S, Fan F and Stewart B G 2023 Modelling of electric field distributions on cable termination defects under DC plus ripples *2023 IEEE Electrical Insulation Conference (EIC)* (IEEE) 1–4